ELSEVIER

Computers and Geotechnics 29 (2002) 279–299

COMPUTERS AND GEOTECHNICS

www.elsevier.com/locate/compgeo

# Strength anisotropy of fiber-reinforced sand

Radoslaw L. Michalowski[a,*], Jan Čermák[b]

[a]*Department of Civil and Environmental Engineering, The University of Michigan, 2340 G.G. Brown Bldg., Ann Arbor, MI 48109-2125, USA*

[b]*Mueser Rutledge Consulting Engineers, New York, USA*

Received 8 May 2001; received in revised form 5 October 2001; accepted 15 October 2001

**Abstract**

The contribution of fibers to the strength of fiber-reinforced soils is very much dependent on the distribution of orientation of the fibers. The fibers in the direction of largest extension contribute most to the strength of the composite, whereas the fibers under compression have an adverse effect on the composite stiffness, and they do not produce an increase in the composite strength. Considering a contribution of a single fiber to the work dissipation during failure of the composite, and integrating this dissipation over all fibers in a composite element, a failure criterion is derived for fiber-reinforced sand with an anisotropic distribution of fiber orientation. A deformation-induced anisotropy was detected in experiments. Specimens with initially isotropic distribution of fiber orientation exhibited a kinematic hardening effect. The evolution of fiber orientation in the deformation process was found to have been the cause of the anisotropic hardening. 

## 1. Introduction

Experimental results gathered over the last 20 years indicate that short fibers mixed into soils can have a noticeable reinforcement effect [1–3]. Description of yielding of reinforced soils has been the subject of research in the context of both traditional reinforcement such as geotextiles, georgid, and metal strips [4–6] and short fiber or filament reinforcement [7–9].

Whether in practical applications or laboratory testing, the distribution of fibers can usually be characterized by a ''preferred'' plane of fiber orientation. In practical applications this plane is associated with the technique of compaction (for instance,

* Corresponding author. Tel.: +1-734-763-2146; fax: +1-734-764-4292.
*E-mail address:* rlmich@umich.edu (R.L. Michalowski).

0266-352X/02/$ - see front matter 
PII: S0266-352X(01)00032-5

rolling of a fiber-reinforced road subgrade), and in laboratory testing it is determined by the specimen preparation technique (vibrating, tamping). The distribution of the fibers determines the anisotropy of the mechanical behavior of reinforced soil. In earlier research [3] it was assumed that only fibers subjected to tension contribute to an increase in soil strength, and the contribution of a single fiber is dependent on its orientation with respect to the principal axes of deformation of the composite. Experimental evidence shown in this paper supports the earlier hypothesis.

Since the distribution of fiber orientation in practical applications is clearly anisotropic, the use of existing isotropic models leads to inaccurate predictions of the strength gain attributed to fibers. For cases where the predominant load is perpendicular to the preferred plane of fiber orientation, isotropic models will, in general, under-predict the benefit from fibers. A technique sometimes referred to as the Hill principle of macrohomogeneity will be used in this paper for predicting an anisotropic gain in strength due to a predetermined distribution of fiber orientation.

An increase in strength of fiber-reinforced soils due to anisotropic hardening is also discussed in this paper. Laboratory experiments show that when fiber-reinforced soil is subjected to large strains, the variation of fiber orientation distribution produces an anisotropic increase in strength. A mechanistic approach to the description of this phenomenon is included in this paper, although no attempt is made at the development of a full constitutive model.

Experimental results from triaxial testing of sand with fibers in a preferred direction are presented first, followed by a mathematical description of strength increase in sand with an anisotropic distribution of fibers. Evolution of the yield condition due to anisotropic hardening is also discussed.

## 2. Triaxial testing

The tests were designed to indicate the role of the inclination of fibers in the increase in soil strength. A hypothesis to be tested suggests that fibers in the direction of maximum extension of a specimen contribute the most to the strength, whereas the fibers subjected to compression do not contribute to strength at all. Hence, in triaxial compression, fibers with a random distribution of orientation should contribute to strength less than horizontal fibers.

The second hypothesis to be tested relates to the behavior of fiber-reinforced sand subjected to large strains. If the contribution of a single fiber to the specimen strength depends on the fiber orientation, then a kinematic (or anisotropic) hardening effect should appear if fiber orientation evolves substantially due to specimen strain.

### *2.1. Sand and fibers tested*

Two sands were used in experiments, one with grains significantly smaller than the fiber diameter, and the second with grains larger than the fiber diameter. Grain size distribution for the two sands is shown in Fig. 1. The material characteristics of the

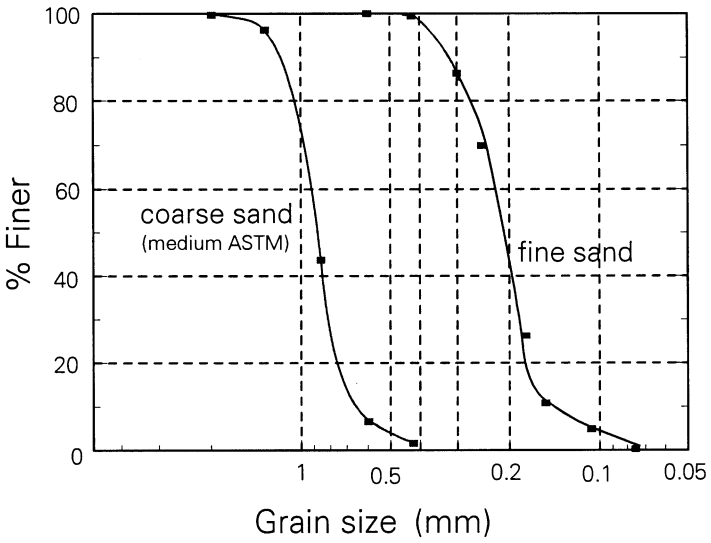


Fig. 1. Grain size distribution for tested sands.

fine sand were: $d_{50}=0.22$ mm, $C_u=1.60$ (coefficient of uniformity), specific gravity $G=2.65$, and the minimum and maximum void ratios $e_{min}=0.52$ and $e_{max}=0.80$, respectively. The parameters of the coarse sand were: $d_{50}=0.89$ mm, $C_u=1.52$, $G=2.65$, $e_{min}=0.56$, and $e_{max}=0.89$.

Two types of fibers were used: monofilament polyamide fibers, 0.3 mm in diameter ($2r$) and 25.4 mm in length ($l$), and galvanized steel fibers of the same size (aspect ratio $\eta = l/2r = 85$). The fiber-sand interface friction angle was determined in a "pull-through" test in a modified shear box apparatus. This angle was found to be pressure-dependent, and it varied from about 18.5° at a normal pressure of 100 kPa to about 15.5° at 800 kPa for polyamide fibers in fine sand. For steel fibers this angle varied from 26 to 21° in the same range of normal stress. The interface friction angle was about the same for fibers in the coarse sand.

### 2.2. Specimen preparation and testing program

Triaxial compression tests were performed on cylindrical fiber-reinforced specimens of 94.5 mm in both height and diameter. All specimens collapsed in a fairly uniform mode without signs of strain localization. The amount of fibers in specimens was described as average fiber concentration $\bar{\rho}$

$$\bar{\rho} = \frac{V_r}{V} \tag{1}$$

where $V_r$ is the volume of fibers in the specimen and $V$ is the volume of the entire specimen. The influence of fiber concentration on the increase of the composite

strength was presented earlier [10], and all specimens here were characterized by $\bar{\rho} = 0.25\%$. Two series of tests were performed, the first one with fine sand and (a) fibers with a randomly distributed orientation, (b) all fibers in the horizontal direction, and (c) all fibers in the vertical direction. Specimens with both polyamide and steel fibers were tested. The second series included an identical program, but with coarse sand. In addition, specimens of fine sand with a large fiber concentration ($\bar{\rho} = 2\%$) were tested at large strains in order to capture the effect of kinematic hardening caused by varying orientation of the fibers.

Specimens with randomly distributed fiber orientation were prepared using a technique earlier described in Michalowski and Zhao [3]. Specimens with all fibers horizontal were prepared by manually placing the fibers in a radial pattern throughout the specimen height; manual placing of fibers was used also for specimens with vertical fibers. All specimens were prepared in molds using dry sand, and they were gently vibrated to the required void ratio of $e = 0.58$ and $e = 0.66$ for the fine and coarse sand, respectively.

The loading process was drained, and it included an isotropic increase in the confining stress to the level of 400 kPa, followed by an increase in the deviatoric loading. This increase was kinematically controlled with a strain rate of $1.7 \times 10^{-3}$ 1/min (or displacement rate of 0.16 mm/min.), and this loading was continued into the post-failure regime.

## 3. Test observations

### 3.1. Small fiber concentration

A small volumetric fiber concentration of $\bar{\rho} = 0.25\%$ was used because of the cumbersome, manual placement of fibers in the specimens with vertical and horizontal distribution of orientation. These tests were not designed to indicate the magnitude of strength increase as a function of fiber concentration, but rather to indicate a qualitative tendency of the reinforcement effect as a function of fiber orientation. This is of interest in developing a model for description of the anisotropic strength of fiber-reinforced soils.

Fig. 2 illustrates the behavior of the fine sand reinforced with polyamide fibers with a vertical orientation, a horizontal orientation, and with a random distribution of orientation. In addition, a stress–strain curve for unreinforced sand is shown. Fig. 3 shows a similar series of tests, but with steel fibers. It is clear that for both, horizontal fibers benefit the strength of the composite the most, while the vertical fibers have an adverse effect on stiffness and provide no strength increase. The increase in strength of specimens with a randomly distributed fiber orientation is very small due to the small concentration used in this test series ($\bar{\rho} = 0.25\%$ by volume). However, the results confirm the hypothesis stated earlier [3] that fibers in compression do not contribute to reinforcement, and may even have an adverse effect. The drop in the strength is marginal, but it is associated with a clear decrease in the initial stiffness.

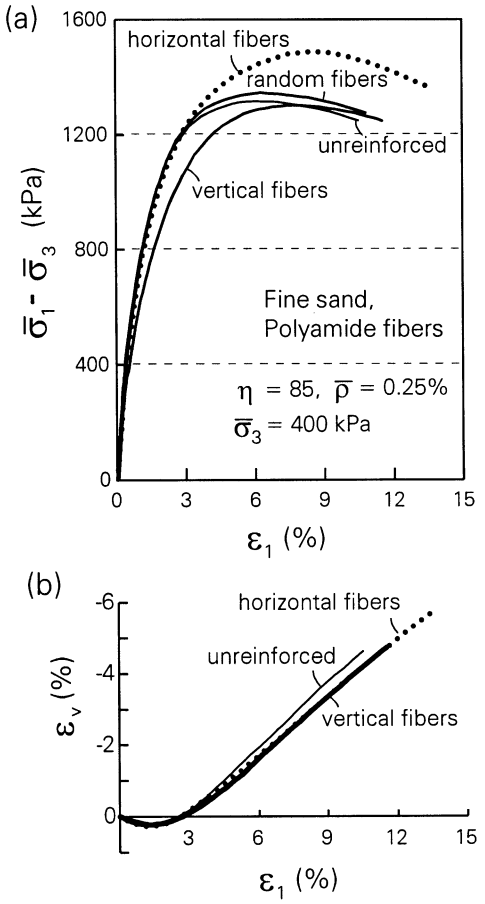


Fig. 2. Fine sand with polyamide fibers: (a) stress–strain behavior, and (b) volumetric strain.

Fibers that contribute most to strength are those with an orientation in the direction of maximum specimen extension. In axisymmetric compression the maximum extension occurs in the horizontal plane; therefore, the contribution of the horizontal fibers is the largest. In a specimen with randomly distributed fibers, a part of the fibers is compressed and a part is subjected to extension (of various intensity); consequently, the overall contribution of these fibers to strength is less than that of horizontal fibers with the same concentration. The increase in strength produced by steel fibers is larger than that produced by polyamide fibers. This is due to a different interface friction angle of the two types of fibers. For steel fibers this angle was found to be in the range of 26–21°, and for polyamide fibers 18.5°–15.5°, with the interface normal stress varying from 100 to 800 kPa (fiber pull-through tests).

A similar reinforcement effect can be identified in coarse sand (Figs. 4 and 5), with the exception that the randomly distributed fibers inhibit dilatancy to a larger degree [compare, for instance, Figs. 2(b) and 4(b)].

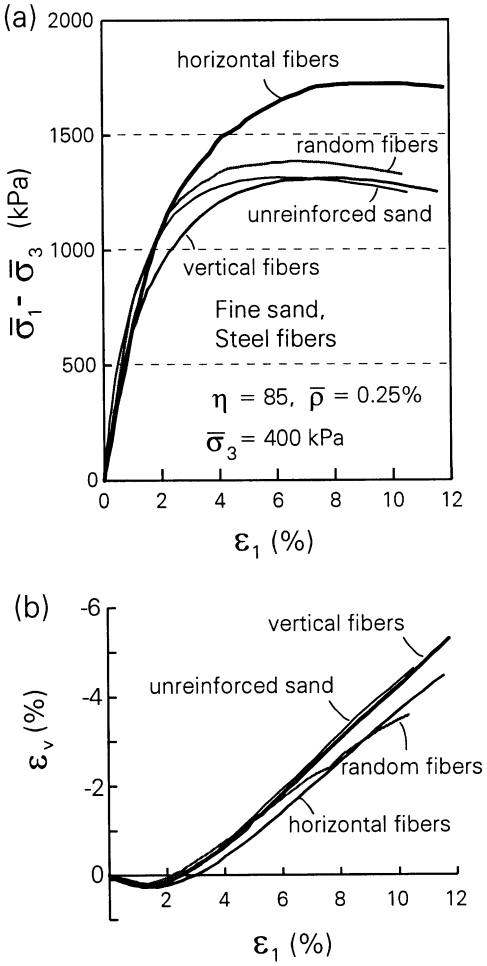


Fig. 3. Fine sand with steel fibers: (a) stress–strain behavior, and (b) volumetric strain.

### 3.2. Large strain of specimens with random fiber orientation

Stress–strain curves for two specimens with a randomly distributed fiber orientation, tested at confining stresses of 300 and 400 kPa, are shown in Fig. 6. The fiber concentration is now 2%, and the specimens are deformed to large strains (although it is a small-strain measure that is used in Fig. 6 on the $\varepsilon_1$axis).

As expected, the increase in strength is now considerably larger as the fiber concentration is increased 8-fold. Also, the dilatancy of the specimens is inhibited to a larger degree [Fig. 6(b)]. The stress–strain curves do not exhibit a peak as, for instance, the curves in Fig. 2 do. Instead, the deviatoric stress first increases with a decreasing first derivative, and it reaches an inflection point at about 25% of specimen vertical strain. Past that point the deviatoric stress increase is associated with an

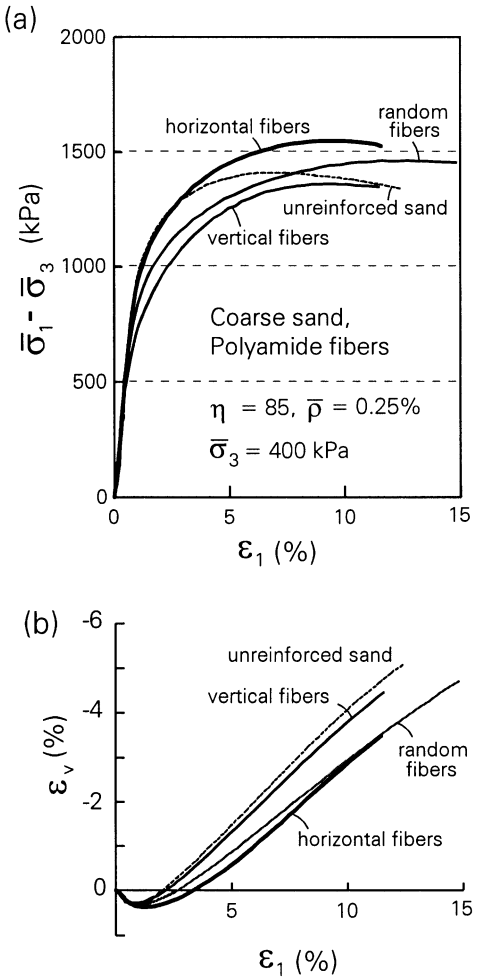


Fig. 4. Coarse sand with polyamide fibers: (a) stress–strain behavior, and (b) volumetric strain.

increase in the first derivative. This is a clear hardening effect and it is seen in both stress–strain curves in Fig. 6(a). The calculation of stress was compensated for the change in the specimen geometry, but strain $\varepsilon_1$ is the engineering (nominal) strain and not the large strain measure. If a natural (logarithmic) measure of strain were to be used, this effect would not be as distinct, as the compressive nominal strain progressively underestimates the true strain.

The hardening effect noticed in the experiments is likely to be caused by the variation of orientation of fibers in the specimen. This hypothesis is consistent with earlier observations indicating that the strength of sand reinforced with fibers with a randomly distributed orientation was smaller than that for a specimen reinforced with horizontal fibers. This hypothesis also will be tested (validated) numerically

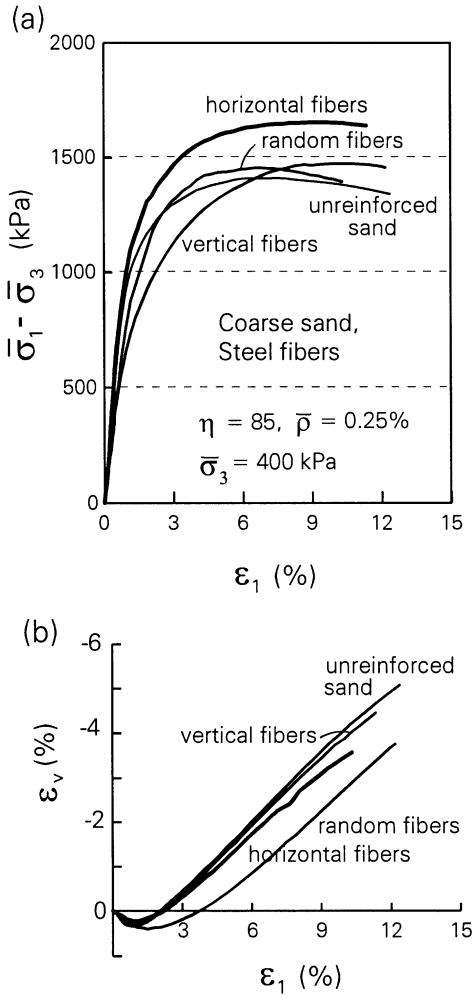


Fig. 5. Coarse sand with steel fibers: (a) stress–strain behavior, and (b) volumetric strain.

where the variation of strength will be simulated as a function of the evolution of fiber orientation in a deformation process.

## 4. Analysis of strength anisotropy of fiber-reinforced sand

Experimental results shown indicate clearly that the strength of fiber-reinforced sand is very much dependent on the distribution of orientation of the fibers. Preparing specimens with an arbitrarily chosen (but well defined) distribution of fiber orientation is a formidable task, therefore only specimens with random and uniform (vertical or horizontal) orientation distribution were tested. Numerical simulations

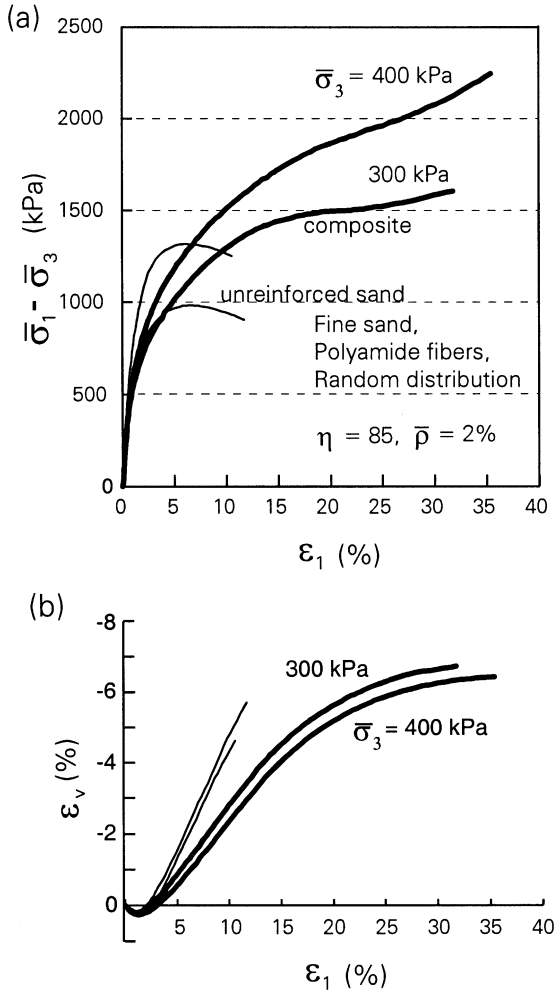


Fig. 6. Kinematic hardening of fine sand with polyamide fibers: (a) stress–strain behavior, and (b) volumetric strain.

will now be used to arrive at a description of strength for different fiber orientation distributions.

### 4.1. Background—isotropic strength

An energy-based homogenization procedure for predicting the strength of a composite with a distribution of fibers uniform in all directions was explained in an earlier paper [3]. A plane-strain deformation of an element of fiber-reinforced soil is considered and the rate of work of external forces acting on that element ($\bar{\sigma}_{ij}$) is required to be equal to the internal work rate (work dissipation). The work dissipation

occurs on the soil-fiber interfaces, and the following general rule for homogenization is used

$$\bar{\sigma}_{ij}\ \dot{\bar{\varepsilon}}_{ij} = \frac{1}{V}\int_V \dot{D}(\dot{\varepsilon}_{ij})\mathrm{d}V \tag{2}$$

where $\bar{\sigma}_{ij}$ is the macroscopic (homogenized) stress on the element, $\dot{\bar{\varepsilon}}_{ij}$ is the average strain rate of the composite, $\dot{D}(\dot{\varepsilon}_{ij})$ is the rate of work dissipation in the element, and $V$ is the volume of the deforming element.

During the deformation process part of the work done by the load is being stored in the system as elastic strain energy and part of the work is dissipated (plastic process). Failure is defined here as the stress state at which the stiffness of the composite drops down to zero. Therefore, as deformation at failure occurs without load increase, strain energy in the system is constant (elastic strain energy rate or increment is equal to zero). Hence, the entire work increment at failure is dissipated.

### 4.2. Distribution of fiber orientation

The distribution of fiber orientation in practical applications of reinforced soil is anisotropic because of the techniques of placement and compaction (rolling) of the soil. In typical construction conditions the horizontal plane is the bedding plane, and the fiber orientation distribution can be described with a function of inclination angle $\theta$ to the horizontal. The fiber concentration now can be represented better as function of the average concentration in Eq. (1) and angle $\theta$. A convenient form of such function was suggested earlier [9] for continuous filament reinforcement, and it is presented here in a slightly different form

$$\rho(\theta) = \bar{\rho}\ \ (A + B|\cos^n\theta|) \tag{3}$$

where $A$, $B$, and $n$ are constant, but only two of them are independent. The average fiber concentration in Eq. (1) must, of course, be equal to

$$\bar{\rho} = \frac{1}{V}\int_V \rho(\theta)\ \ \mathrm{d}V \tag{4}$$

After integrating the distribution in Eq. (3), constant $B$ can be found as a function of $A$ and $n$

$$B = \frac{1 - A}{\int_0^{\pi/2}\cos^{n+1}\theta\ \ \mathrm{d}\theta} \tag{5}$$

If $n$ is a positive even integer then

$$B = (1 - A)\ \ \frac{(1+n)!!}{n!!} \tag{6}$$

where !! is the double factorial [$n!! = 2\ 4\ 6 \ldots n$ and $(n+1)!! = 3\ 5\ 7 \ldots (n+1)$]. For a practical case where no vertical fibers are present, coefficient $A = 0$. Such a distribution is illustrated in Fig. 7, and more examples are shown in Fig. 8. The distribution in Eq. (3) becomes isotropic when $B = 0$ [which also implies that $A = 1$, see Eq. (5)].

### 4.3. Rate of work dissipation during failure

The fiber-sand interface is assumed here to be of a frictional nature, and work dissipation occurs during sliding of the fibers in the sand matrix or during plastic deformation of the fibers after the fiber stress has reached the yield point. The rate of work dissipation for a single fiber was presented earlier [3] and so was the work dissipation for the composite with a uniform distribution of fiber orientation (isotropic material). In order to integrate the work dissipation in composite with an anisotropic distribution of fibers, a spherical integration space is introduced, Fig. 9 (only $\frac{1}{4}$ shown in the figure). Deformation of a composite element, Fig. 10, is then transformed into a spherical integration space where all fibers are moved to the space origin in a parallel manner. Such an operation is admissible since the dissipation depends only on the fiber orientation and not on its specific location in the specimen.

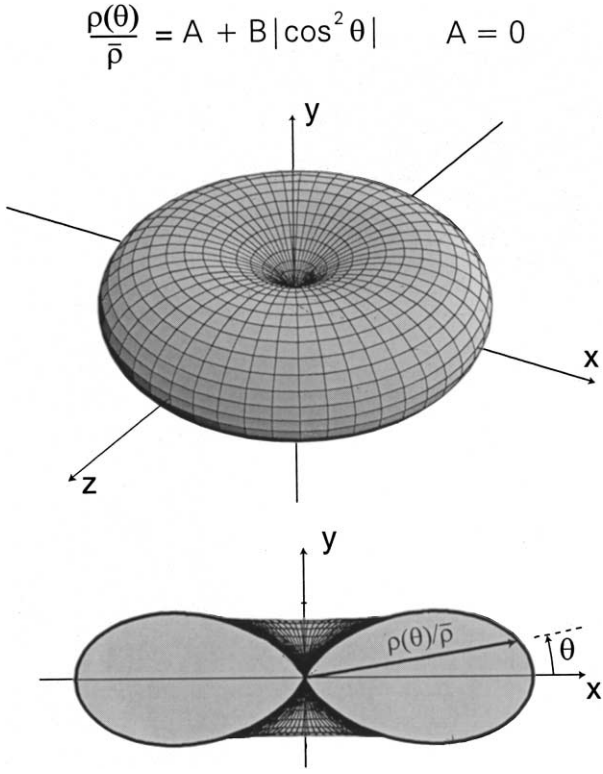


Fig. 7. Axisymmetric cosine fiber orientation distribution.

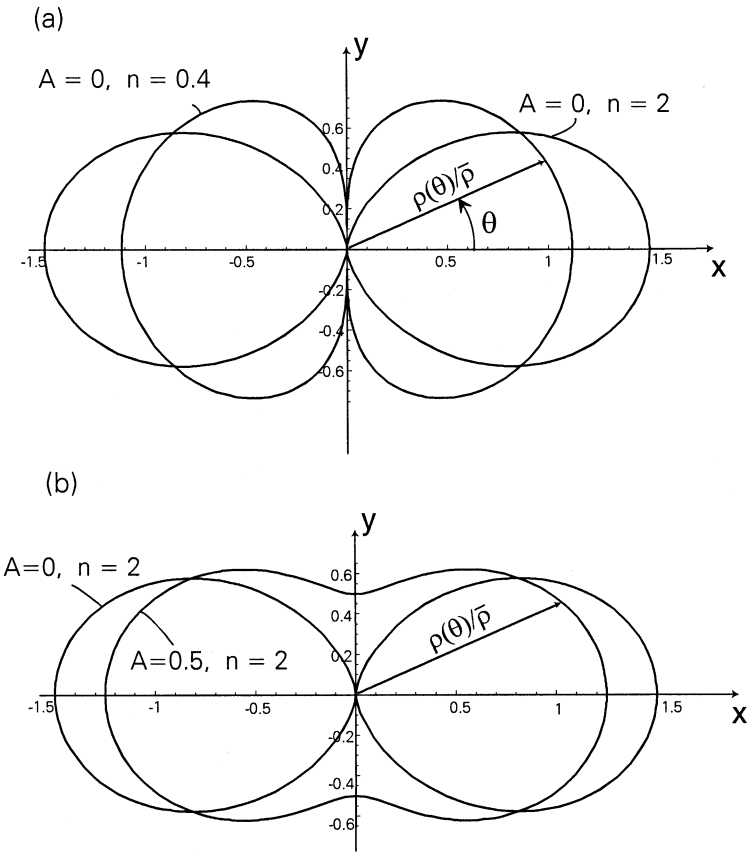


Fig. 8. Fiber orientation distribution.

Deformation of the matrix in the element shown in Fig. 10 is governed by the Mohr–Coulomb yield condition and the normality rule. Consequently, in a plane-strain compression process with the principal compressive strain rate in the direction $y'$, Fig. 9, the fibers between planes OBCO and OECO are in the tensile regime, whereas above and below these planes fibers are subjected to compression. The angle of inclination of these planes was found earlier [9] as

$$\theta_0 = \pm\left(\frac{\pi}{4} + \frac{\varphi}{2}\right) \tag{7}$$

where is the internal friction angle of the sand matrix. Since fibers subjected to compression do not contribute to strength as proved by experiments (possibly because of kinking and buckling), the dissipation needs to be integrated only for fibers in the range between planes OBCO and OECO. However, the distribution of fiber orientation does not need to be symmetric with respect to plane $y'Oz'$, i.e. axes $xyz$ in Fig. 7(a), in general, do not coincide with axes $x'y'z'$ in the integration space

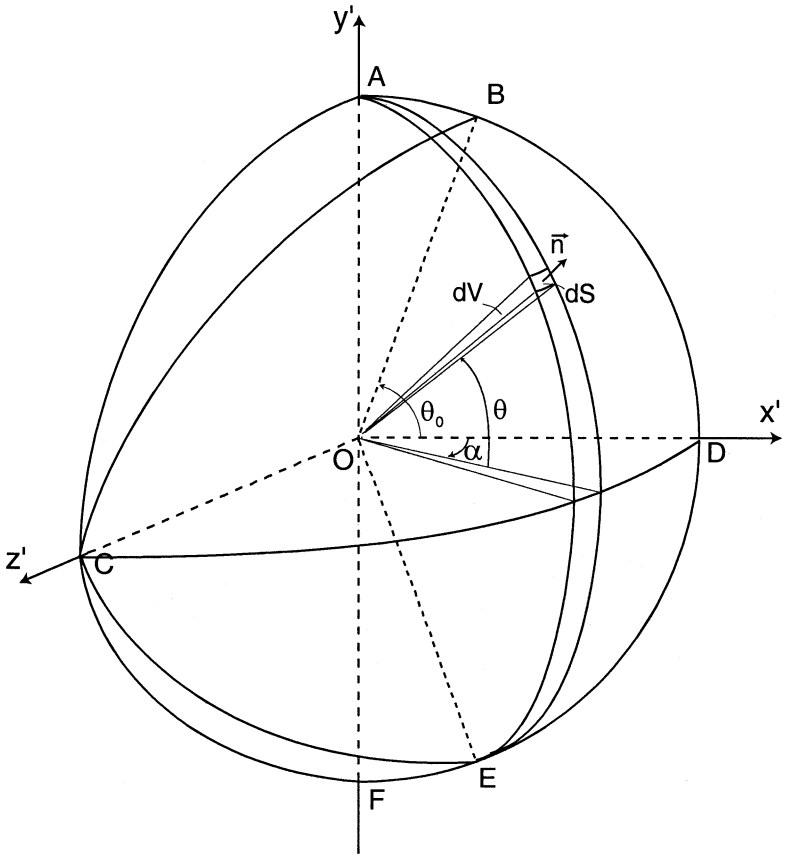


Fig. 9. Integration space.

(Fig. 9). Angle $\theta$ is measured counterclockwise from axis $x'$ in the integration space, and deviation angle ω in plane $x'y'$ is introduced (Fig. 10); this angle describes the angle of inclination of the bedding (preferred orientation) plane to the horizontal ($x'Oz'$) plane. For the purpose of integration, the corresponding angle of deviation as a function of angle $\alpha$ (Fig. 9) was determined to be

$$\omega^* = \tan^{-1}(\cos\alpha \ \tan\omega) \tag{8}$$

and the distribution of fiber orientation in Eq. (3) now takes the form

$$\rho(\theta) \ = \ \bar{\rho} \ [A + B|\cos^n(\theta - \omega^*)|] \tag{9}$$

Following earlier developments [3,9], the rate of work dissipation with fibers slipping in a deforming element is derived as

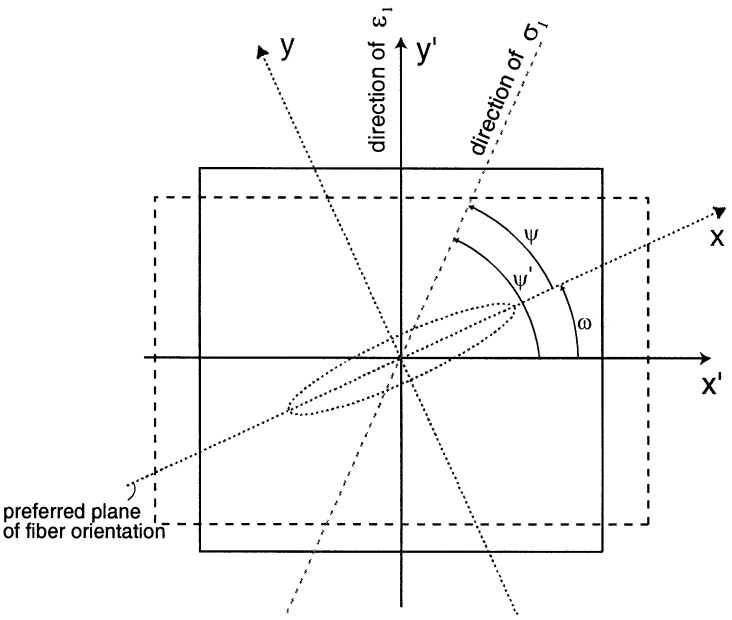


Fig. 10. Plane strain deformation of a composite element.

$$\dot{D}(\dot{\varepsilon}_{ij}) = \frac{1}{\pi}\eta\tan\varphi_{\mathrm{w}}\ p\ \dot{\bar{\varepsilon}}_1 \int_0^{\pi/2}\int_{-\theta_0^*}^{\theta_0^*} \rho(\theta)\ [K_{\mathrm{p}}\cos^2\alpha\ \cos^2\theta - \sin^2\theta]\cos\theta \mathrm{d}\theta\mathrm{d}\alpha \tag{10}$$

and for fibers in a plastic flow (rupture) mode

$$\dot{D}(\dot{\varepsilon}_{ij}) = \frac{\sigma_0}{\pi}\left(1 - \frac{1}{4\eta\, p\tan\varphi_w}\frac{\sigma_0}{}\right)\ \dot{\bar{\varepsilon}}_1 \int_0^{\pi/2}\int_{-\theta_0^*}^{\theta_0^*} \rho(\theta)\ [K_p\cos^2\alpha\ \cos^2\theta - \sin^2\theta]\cos\theta \mathrm{d}\theta\mathrm{d}\alpha \tag{11}$$

where $\eta$ is the aspect ratio of the fibers, $\varphi_w$ is the sand-fiber interface friction angle, $\sigma_0$ is the yield point of the fibers, $p$ is given in Eq. (13), and $\dot{\bar{\varepsilon}}_1$ is the composite major principal strain rate ($\dot{\bar{\varepsilon}}_1 = \dot{\bar{\varepsilon}}_{y'}$). The distribution of fiber orientation is given in Eq. (9), coefficient $K_{\mathrm{p}} = \tan^2(\pi/4 + \varphi/2)$, and $\theta_0^* = \tan^{-1}(\cos\alpha\ \tan\theta)$.

### 4.4. Anisotropic failure analysis

The failure criterion in sought in the form

$$f = R - F(p, \psi) = 0 \tag{12}$$

where $R$ and $p$ are in-plane invariants of the macroscopic stress state, and $\psi$ is the angle of inclination of the composite major principal stress to axis $x$

$$R = \sqrt{\frac{(\bar{\sigma}_x - \bar{\sigma}_y)^2}{4} + \bar{\tau}_{xy}^2}, \qquad p = \frac{\bar{\sigma}_x + \bar{\sigma}_y}{2} \tag{13}$$

We now consider a plane strain deformation of an element in Fig. 10. Axes $x'$ and $y'$ are the principal axes of strain rate $\dot{\bar{\varepsilon}}_{ij}$, but, because the composite is anisotropic, they are not necessarily the principal axes of macroscopic stress $\bar{\sigma}_{ij}$. Hence, the homogenization principle in Eq. (2) can be rewritten as

$$\bar{\sigma}_{x'}\dot{\bar{\varepsilon}}_{x'} + \bar{\sigma}_{y'}\dot{\bar{\varepsilon}}_{y'} + 2\bar{\tau}_{x'y'}\dot{\bar{\varepsilon}}_{x'y'} = \dot{D}(\dot{\varepsilon}_{ij}) \tag{14}$$

Now introducing stress parameter $q'$

$$q' = \frac{\bar{\sigma}_{x'} - \bar{\sigma}_{y'}}{2} = R \quad \cos 2\psi' \tag{15}$$

(see Fig. 10 for $\psi'$) and noting that $\dot{\bar{\varepsilon}}_{x'y'} = 0$, Eq. (14) can be written as

$$q'(\dot{\bar{\varepsilon}}_{x'} - \dot{\bar{\varepsilon}}_{y'}) + p(\dot{\bar{\varepsilon}}_{x'} + \dot{\bar{\varepsilon}}_{y'}) = \dot{D}(\dot{\varepsilon}_{ij}) \tag{16}$$

Considering that for a plane strain of Mohr–Coulomb material governed by the normality rule we have $\dot{\varepsilon}_{x'}/\dot{\varepsilon}_{y'} = \dot{\varepsilon}_3/\dot{\varepsilon}_1 = -K_\mathrm{p}$ (we also assume $\dot{\bar{\varepsilon}}_3/\dot{\bar{\varepsilon}}_1 = -K_\mathrm{p}$), and noting the relation between $q'$ and $R$ in Eq. (15), one can transform Eq. (16) into

$$R = \frac{\dot{D}(\sigma_{ij})/\dot{\bar{\varepsilon}}_1 - p(1 - K_\mathrm{p})}{1 + K_\mathrm{p}} \quad \frac{\cos 2\psi}{\cos 2(\psi + \omega)} \tag{17}$$

The expression on the right-hand side of Eq. (17) represents function $F(p, \psi)$ in Eq. (12). Finding the failure criterion for fiber-reinforced sand with an anisotropic distribution of fiber orientation entails minimization of $R$ in Eq. (17) for given $p$ and $\psi$, with deviation angle $\omega$ being a variable.

There may be two disputable issues in the homogenization concept presented here. The first one is related to application of the normality rule to the frictional matrix of the composite, and the second one has to do with the assumption that the principal directions of composite deformation follow the principal directions of the matrix strain. The flow rule associated with the Mohr–Coulomb yield condition has been contested in the literature as it leads typically to volumetric strain larger than laboratory observations suggest. Therefore, application of normality rule may lead to some overestimation of the true composite strength. Laboratory tests with isotropic fiber-reinforced sand [3] indicate that the associative rule of plasticity applied to composite matrix yields a fairly accurate description of the failure criterion of the composite strength. Because of these laboratory results and mathematical convenience, the normality rule was applied to the matrix material.

The second approximation that requires a comment is the assumption that the deformation of the composite coincides with the deformation of the matrix (of

course, the principal directions of the stress state in the matrix and in the composite do not coincide). This statement does not indicate that addition of fibers to the matrix does not alter composite deformation. If two representative elements, one containing matrix material only and the other one comprised of the composite, are loaded to failure along the same load path, the deformation response of the two elements, in general, will be different in that the principal directions of the strain will differ for the two elements.

While the assumption that the macroscopic deformation of the composite is governed by the same rule as the deformation of the matrix can be disputed, it is not unreasonable. The volumetric content of the fibers in the composite is small (less than 1% in practical applications), and they are not likely to affect the average deformation pattern of the matrix to a significant degree. The average stress state in the composite, of course, can differ significantly from the stress state in the matrix.

### 4.5. Example of an anisotropic failure criterion for reinforced sand

The distribution function in Eq. (3) is adopted here with $A=0$ and $n=2$ [Fig. 8(a)]. This distribution assumes a convenient form

$$\rho(\theta) = \bar{\rho}\frac{3}{2}\cos^2\theta \tag{18}$$

This is a realistic distribution with the horizontal ($\theta=0$) being the bedding plane, and with no fibers in the vertical direction. The remaining parameters necessary to define the failure criterion are: average fiber concentration $\bar{\rho}=5\%$ ($\bar{\rho}=0.05$), fiber aspect ratio $\eta=250$, fiber yield point $\sigma_0=50$ MPa, internal friction angle of sand $\varphi=36^\circ$, and sand-fiber interface friction angle $\varphi_w=27^\circ$. In order to present a very distinct increase of strength, the fiber concentration ($\bar{\rho}$) and aspect ratio ($\eta$) were taken larger than those used typically in practical applications (and in experiments presented in this paper).

The minimization scheme described in the previous subsection was used to arrive at the shear strength of the composite, and it is presented in Fig. 11. The inner conical surface represents the strength of sand (Mohr–Coulomb function). Shear strength $R$ is depicted by the radius of the conical surface ($R=\sqrt{q^2+\tau_{xy}^2}$; $q=(\bar{\sigma}_x-\bar{\sigma}_y)/2$). As the inner surface is axisymmetric, strength $R$ is independent of orientation, and this surface represents the isotropic strength. The outer surface in Fig. 11 was determined for the composite by minimizing shear strength $R$ in Eq. (17). Clearly, this surface is not axisymmetric, which indicates that the composite is anisotropic.

The yield surface for the fiber-reinforced sand has two sections [Fig. 11(b)]: a linear conical surface associated with pure slip of fibers in the sand matrix, and a nonlinear conical surface associated with the rupture of fibers. Theoretically, rupture of fibers can occur when the fiber yield point is low and the confining stress is very large, or when the aspect ratio of the fibers is very large. No rupture of polyamide,

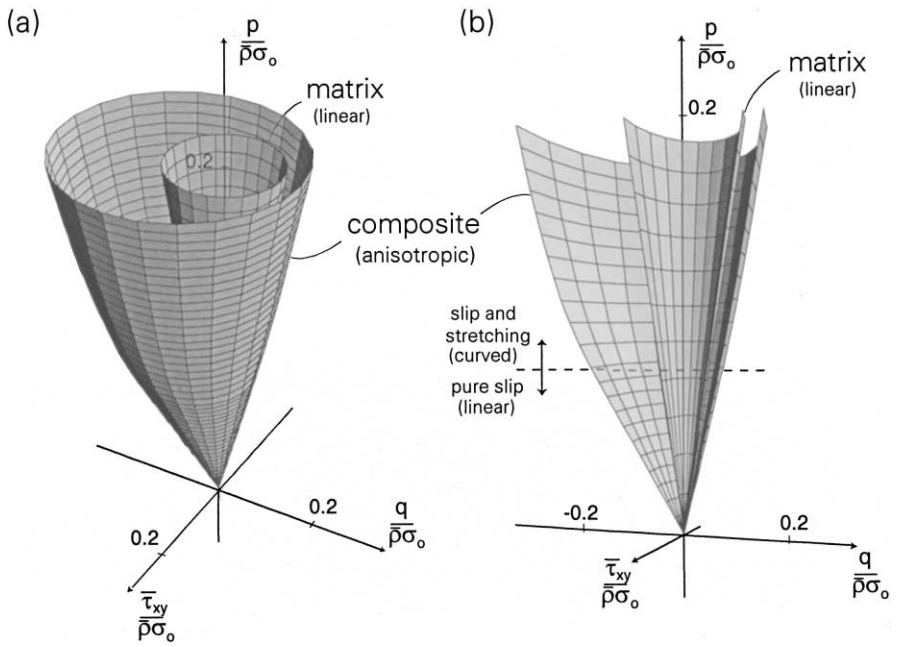


Fig. 11. Anisotropic failure condition for fiber-reinforced sand: (a) failure surface, and (b) cross-section of the failure surface.

steel or glass fibers was observed in experiments [2,3], and a practical case of composite failure is one with the fiber slip. The two sections of the surface were determined by minimizing $R$ in Eq. (17) with dissipation in either Eq. (10) or (11). The surface in Fig. 11 can be used directly in calculations of plastic stress fields in boundary value problems [11].

### 4.6. Kinematic hardening and induced anisotropy

A description of anisotropic fiber-reinforced sand was shown in the previous sections. Here, an attempt is made to explain the hardening process seen in Fig. 6. The specimens in Fig. 6 were originally isotropic with a distribution of fibers as presented in Fig. 12(a). However, during triaxial compression the distribution varied, as indicated in Fig. 12(b). This distribution is now the source of anisotropy (induced anisotropy), and the process can be classified as kinematic hardening. The ellipsoidal distribution of fiber orientation can be described as

$$\rho(\theta) = \sqrt{\frac{a^2}{1 - \sin^2\theta(1 - a^2/b^2)}} \tag{19}$$

where $a$ and $b$ are the semi-axes of the ellipsoid [Fig. 12(b)], and the distribution is isotropic when $a = b$. This varying distribution in Fig. 12 [and Eq. (19)] is distinctly

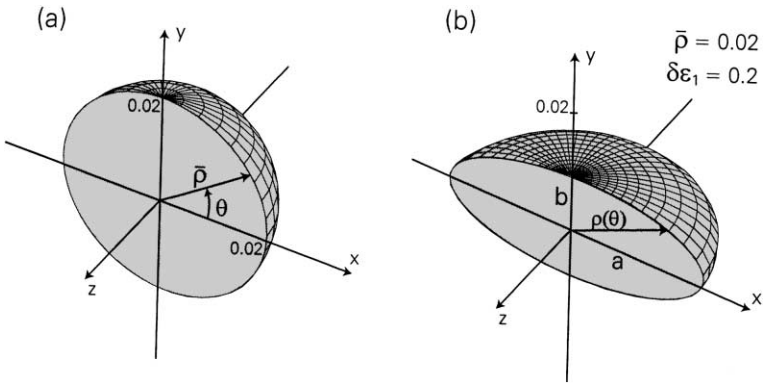


Fig. 12. Variation of fiber orientation distribution; (a) original distribution, (b) distribution after 20% of major principal strain.

different from the earlier distribution introduced in Eq. (3) for the purpose of describing inherent anisotropy. The evolution of the distribution in Eq. (19) was found to be more straightforward in its interpretation, and therefore it was used in calculations of kinematic hardening.

Considering deformation governed by the normality rule associated with the Mohr-Coulomb yield condition, a change in inclination of a single fiber, Fig. 13, can be described as

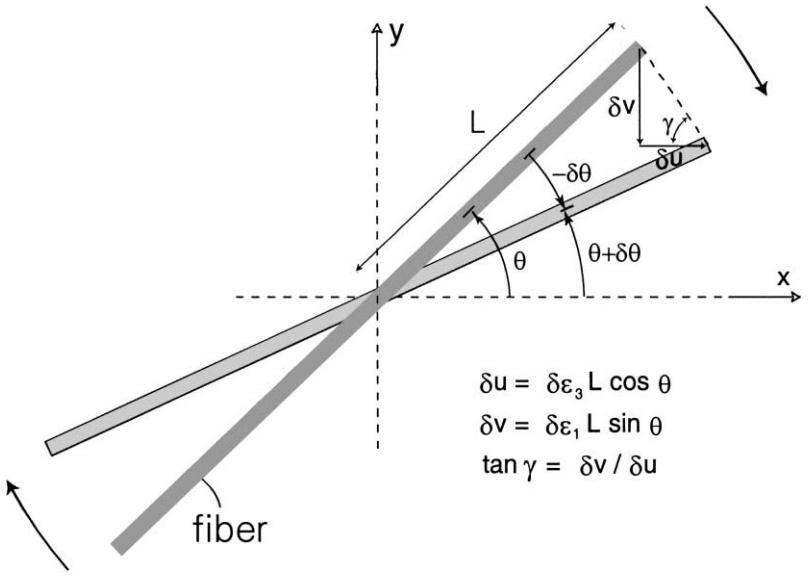


Fig. 13. Variation of orientation of a single fiber during a composite deformation process.

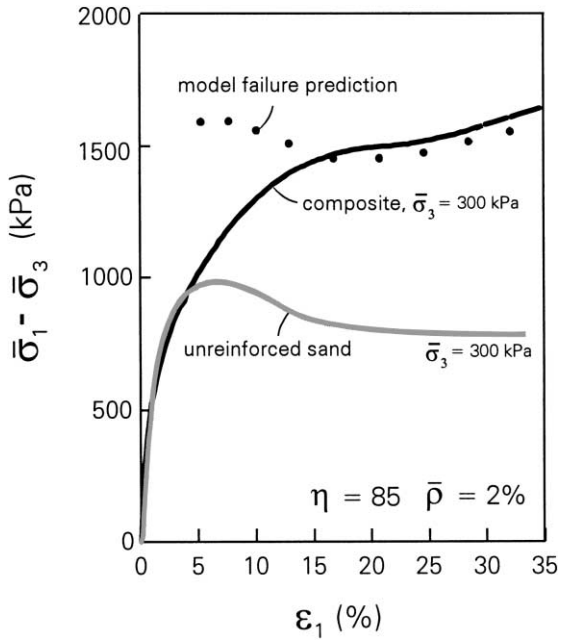


Fig. 14. Predicted deviatoric stress increase.

$$\delta\theta = -\tan^{-1}\left[\frac{\delta\bar{\varepsilon}_1 \sin(\gamma+\theta)\sqrt{\sin^2\theta + \frac{K_p^2}{4}\cos^2\theta}}{1 + \delta\bar{\varepsilon}_1 \cos(\gamma+\theta)\sqrt{\sin^2\theta + \frac{K_p^2}{4}\cos^2\theta}}\right] \tag{20}$$

where $\gamma = \tan^{-1}(2\tan\theta/K_p)$ and $K_p = \tan^2(\pi/4 + \varphi/2)$.

The evolution in parameter $a$ in Eq. (19) can be calculated from the fiber inclination change in Eq. (20), and the change in parameter $b$ can be found from the requirement that the average fiber concentration, Eq. (1), has not changed in the deformation process (only the fiber orientation has changed). Consequently, the strength of the fiber-reinforced sand can be calculated at different stages of deformation characterized by a changing distribution of fiber orientation. Such calculations were performed, and the results are superimposed over the experimental stress–strain relation in Fig. 14. The prediction of stress in the early stage of the process is not accurate, since the sand was modeled as rigid-plastic, and the gradual mobilization of stress was not simulated. The initial drop in predicted stress is associated with the softening of the sand. However, after about 15% of strain, the evolution of fiber distribution leads to a clear hardening effect. This is a kinematic (or anisotropic) hardening effect, where the composite becomes stronger in the direction of the stress path, but it becomes weaker in the transverse direction.

This analysis was to indicate the importance of the variation in the fiber distribution, and to validate the hypothesis that the evolution in this distribution is responsible for the hardening effect. This was not an attempt at developing a full constitutive model of the composite.

## 5. Conclusions

A series of experimental tests was performed on specimens of sand reinforced with polyamide and steel fibers. Cylindrical specimens were subjected to drained triaxial compression. Three distributions of fibers were tested: random orientation, all fibers in the vertical direction, and all fibers in the horizontal direction. The contribution of the fibers to the composite strength is the largest when they are placed in the direction of largest extension of the composite (here, horizontal). Vertical fibers in triaxial testing were subjected to compression; they had an adverse effect on the initial stiffness of the composite, and they did not contribute to any strength increase. Specimens with a random distribution of fibers exhibited a smaller increase in strength than those with horizontal fibers, because a portion of randomly distributed fibers is subjected to compression.

The strength (failure condition) of sand with anisotropically distributed fibers was described using a homogenization approach. The shear strength under plane-strain conditions was described by a function dependent on the in-plane mean stress and the inclination of the major principal stress. This strength can be illustrated as a convex conical surface in a stress space. The failure criterion derived can be applied directly in methods for solving stability problems for fiber-reinforced sand.

The kinematic hardening effect was detected at large strain in experiments with a 2% fiber concentration. This effect is caused by the evolution of the fiber orientation distribution during composite deformation. No attempt was made at developing a full constitutive model of the composite, but a simulation of the triaxial compression indicated that the kinematic hardening effect indeed can be captured through the evolution of the fiber orientation distribution.

## Acknowledgements

The research presented in this paper was supported by the National Science Foundation, Grant No. CMS-0096167. This support is greatly appreciated.

## References

[1] Gray DH, Ohashi H. Mechanics of fiber reinforcement in sand. J Geot Eng 1983;109:335–53.
[2] Maher MH, Gray DH. Static response of sands reinforced with randomly distributed fibers. J Geot Eng 1990;116(11):1661–77.
[3] Michalowski RL, Zhao A. Failure of fiber-reinforced granular soils. J Geot Geoenv Engrg 1996; 122(3):226–34.

[4] De Buhan P, Mangiavacchi R, Nova R, Pellegrini G, Salençon J. Yield design of reinforced earth walls by homogenization method. Géotechnique 1989;39(2):189–201.
[5] Michalowski RL, Zhao A. Continuum vs. structural approach to stability of reinforced soil. J Geotech Engrg 1995;121(2):152–62.
[6] Sawicki A. Mechanics of Reinforced Soils. Rotterdam: Balkema, 2000.
[7] Di Prisco C, Nova R. A constitutive model for soil reinforced by continuous threads. Geotextiles and Geomembranes 1993;12:161–78.
[8] Verzura L. A macroscopic strength criterion for continuous thread reinforced soil. Mech Research Com 1994;21(4):353–9.
[9] Michalowski RL. Limit stress for granular composites reinforced with continuous filaments. J Eng Mech 1997;123(8):852–9.
[10] Michalowski RL, Čermák J. Triaxial compression of sand with randomly distributed fibers. J Geot Geoenv Eng (in press).
[11] Booker JR, Davis EH. A general treatment of plastic anisotropy under conditions of plane strain. J Mech Phys Solids 1972;20:239–50.